Frontiers in Heat and Mass Transfer (FHMT), 20, 22 (2023)
DOI: 10.5098/hmt.20.22

Global Digital Central
ISSN: 2151-8629

Frontiers in Heat and Mass Transfer

Available at www.ThermalFluidsCentral.org

NUMERICAL CALCULATION OF REVERSE STARTUP OF A SMALL RADIAL VANE PUMP

Feng-Lin Zhou[a], Kai-Yuan Zhang[a], Liang Cheng[b,†], Hai-Bing Cai[c], Yu-Liang Zhang[b], Min-Feng Lv[d]

[a] *School of Mechanical Engineering, Hunan University of Technology, Zhuzhou, Hunan, 412007, China*
[b] *College of Mechanical Engineering, Quzhou University, Quzhou, Zhejiang, 324000, China*
[c] *Zhejiang Testing & Inspection Institute for Mechanical and Electrical Products Quality Co., Ltd., Hangzhou, Zhejiang, 310014, China*
[d] *Zhejiang Zhigao Machinery Co., Ltd., Quzhou, Zhejiang, 324024, China*

ABSTRACT

In order to grasp the reverse startup characteristics of a small radial vane pump in the case of misoperation, a circulation piping system that includes the pump is established. Numerical simulation of the full three-dimensional unsteady incompressible viscous flow is performed based on the slip-grid technique and user-defined functions (UDF). According to the results, the static pressure fluctuation is small at the inlet of the centrifugal pump during the reverse startup, which differs significantly from the forward startup. Compared to the impeller rotational speed, the time required for the shaft power, head and flow curves to reach stability is lagged, with the largest lag being shaft power, followed by head and the smallest flow rate. During the startup, the region where the turbulent kinetic energy mainly occurs changes from the outlet of the volute to the flow path of the impeller. There is no turbulent dissipation rate near the leading edge of the blade; In the early stage of the reverse startup, the similar laws of centrifugal pumps are obviously not applicable. In the later stages of the startup, the similitude law can be basically applied to the performance prediction of centrifugal pumps.

Keywords: *Radial type, Centrifugal pump, Reverse rotation, Startup, Numerical simulation*

1. INTRODUCTION

Centrifugal pump is a very widely used radial type vane pump, and its startup process is essential. Until now, a number of scholars have conducted relevant studies on this topic. Tsukamoto *et al*. (1982) investigated the normal startup process of a centrifugal pump by experiments, they found that the impulse pressure and the delay around the vane ring volume were the main causes of the difference between transient and quasi-steady state. Lefebvre *et al*. (1995) experimentally studied the acceleration process of a mixed-flow pump under different situations and found that the quasi-steady-state assumption was not applicable to the transient performance prediction of the pump. Thanapandi *et al*. (1995) experimentally found that the conventional transient startup process is satisfying the quasi-steady-state assumption. Dazin *et al*. (2007) found that the transient effect during startup is not only related to the magnitude of acceleration and flow, but also to the evolution of the flow field. Li *et al*. (2010) performed startup calculation of a centrifugal pump with dynamic grid method and found that the numerical simulation method was completely feasible and reliable. Wu *et al*. (2006) conducted experiments for the rapid startup of centrifugal pumps and found that the transient characteristics of the initial startup stage were more significant compared to other stages. Hu *et al*. (2005) compared the experimental results of rapid startup of a centrifugal pump with the results under the quasi-steady-state assumption, and also found that there was an obvious transient effect in the initial stage of startup, but the transient performance after startup stabilization was basically the same as the steady-state performance. Wang *et al*. (2008) used the dynamic grid method and the quasi-steady-state assumption to simulate the two-dimensional centrifugal pump startup process respectively, and qualitatively described the transient effects of the centrifugal pump startup process by comparatively analyzing the results of the two simulations. Chen *et al*. (2006) carried out startup experiments on centrifugal pumps at different valve openings, established the theoretical head calculation formula under unstable working conditions by analyzing the flow history, and modified the test head. In addition, a number of other transient characteristics have been studied in depth. In a previous study by the authors (Zhang *et al*., 2017), the authors carried out the fast startup characteristics of a centrifugal pump under normal conditions, i.e. in forward rotation. The transient flow behavior inside pumps is the fundamental reason for hydraulic performance (Chen *et al*., 2022; Chen and Zhang *et al*., 2022).

However, in practice, there are often cases of operator error, i.e., reversing the startup. Until now, research on the reverse startup of centrifugal pumps has not been seen. In order to grasp this characteristic, a circulation pipeline is built in this paper, which includes the pump model, and the entire circulation pipeline system is calculated numerically to obtain the characteristics of the pump model's reverse startup. The entire calculation process is self-coupled without providing boundary conditions for the pump model inlet and outlet.

2. NUMERICAL SIMULATION METHODS

2.1 Physical Model

The pump used for numerical calculations is a low specific speed centrifugal pump with a specific speed of 45, which is the same as the model in the reference (Zhang *et al*., 2017). The design parameters are: flow rate is 6 m^3/h, head is 8 m, rotation speed is 1450 r/min. The suction diameter and discharge diameter of pump are respectively

† *Corresponding author. Email: chengliang@qzc.edu.cn*

Global Digital Central
ISSN: 2151-8629

50mm and 40mm. The blade number is 5, the impeller diameter is 160mm. The blade angles at inlet and outlet are 25°. The inlet width and outlet width are respectively 20mm and 10mm. The structure of the model pump is shown in Fig. 1.

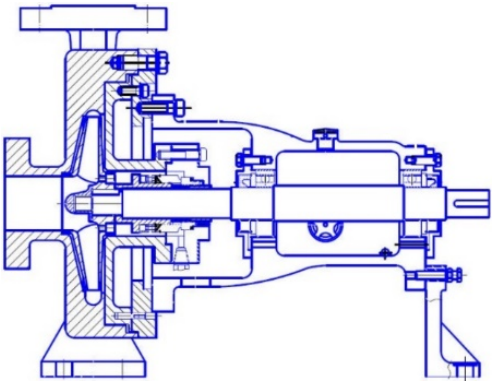

Fig. 1 Structural diagram of model pump

2.2 Governing Equations

The turbulence calculations performed in this study is the RNG k-ε dual equation model to make the Reynolds mean equation closed (Yakhot *et al*., 1986). The RNG k-ε turbulence model including the influence of high strain rate and large curvature overflowing has been verified that it is suitable to simulate the flow inside a pump. The forms are as follows

$$\rho\frac{dk}{dt}=\frac{\partial}{\partial x_j}\left(\alpha_k\mu_{\text{eff}}\frac{\partial k}{\partial x_j}\right)+2\mu_t\overline{\boldsymbol{S}}_{ij}\frac{\partial\overline{u}_i}{\partial x_j}-\rho\varepsilon \tag{1}$$

$$\rho\frac{\mathrm{d}\varepsilon}{\mathrm{d}t}=\frac{\partial}{\partial x_j}\left(\alpha_\varepsilon\mu_{\text{eff}}\frac{\partial\varepsilon}{\partial x_j}\right)+2C_{1\varepsilon}\frac{\varepsilon}{k}v_t\overline{\boldsymbol{S}}_{ij}\frac{\partial\overline{u}_i}{\partial x_j}-C_{2\varepsilon}\rho\frac{\varepsilon^2}{k}-R \tag{2}$$

where $\overline{\boldsymbol{S}}_{ij}=\frac{1}{2}\left(\frac{\partial\overline{u}_i}{\partial x_j}+\frac{\partial\overline{u}_j}{\partial x_i}\right)$, $\mu_{\text{eff}}=\mu+\mu_t$, $\mu_t=C_\mu\frac{k^2}{\varepsilon}$, $\overline{\boldsymbol{S}}_{ij}$ is the strain rate tensor, and R is the additional source term in the ε equation, representing the effect of the average strain rate ε. The expression is

$$R=\frac{C_\mu\eta^3\left(1-\eta/\eta_0\right)}{1+\beta\eta^3}\frac{\varepsilon^2}{k},\eta=Sk/\varepsilon \tag{3}$$

The model parameters in the above equation are: C_μ=0.0845, $C_{1\varepsilon}$=1.42, $C_{2\varepsilon}$=1.68, α_k=1.0, α_ε=0.769, β=0.012, η_0=4.38.

2.3 Computational Domain and Mesh

The circulatory pipeline system built in this study is shown in Fig. 2, and it is fully consistent with that in the reference (Zhang *et al*., 2017). The bottom of the water tank is square, and the size of each section is 500×500×1000mm. The top of the tank is set to a constant atmospheric pressure so that it is exactly the same as the actual situation to get more accurate results. In this study, the valve throat diameter is set to 10 mm. Under the design rotational speed and reversal situation, the calculated steady flow rate of the pipeline is 4.3388m^3/h; While in the forward rotation situation, the steady flow rate of the pipeline system is 4.3337m^3/h (Zhang *et al*., 2017). The difference between the two is caused by the difference in flow loss during forward and reversal rotation. Finally the total number of meshes in the entire computational domain is 1841410. The number of meshes in the impeller region is 616018, and the number of meshes in the volute region is 383233, as shown in Fig. 3, with good mesh quality.

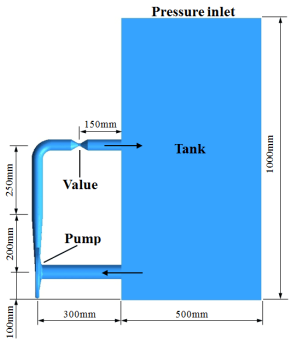

Fig. 2 Circulation pipeline system (Zhang *et al*., 2017)

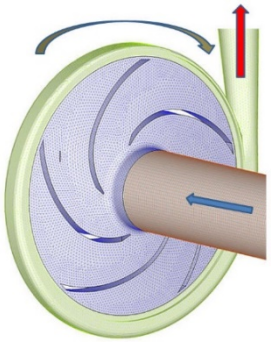

Fig. 3 Impeller meshes

2.4 Numerical Solution

The commercial software FLUENT6.3 based on the finite volume method is used for the numerical calculation of the full three-dimensional incompressible unsteady viscous fluid. The rotor-stator interaction between the impeller and volute is achieved by the slip grid technique. In the process of the reverse startup, the rising rotational speed of the pump still adopts the exponential law. The expression is

$$n=n_{\max}\left(1-e^{-t/t_0}\right) \tag{4}$$

where $n_{\max}$ 1450r/min and t_0=0.15s.

No-slip boundary conditions are used at the wall, and the standard wall function method is used in the low Reynolds number region near the wall to deal with the problems caused by the high Reynolds number turbulence model. The coupling of velocity and pressure is achieved using the SIMPLE method. The default under-relaxation factors are used for all variables in the iterative calculations. The time step is taken as 0.0001s, and the startup time is 1.0s. The maximum number of iterations in each time step is set to 200 to ensure absolute convergence in each time step (in fact, convergence is achieved in a few dozen iterations in each time step).

3. RESULTS AND DISCUSSIONS

3.1 External Characteristics

Figure 4 shows the comparison between the impeller speed curve and the transient pressure curves at the inlet and outlet of the centrifugal pump during the reverse startup test. Here, Fig. 4 (a) shows the comparison between the rotational speed and the static pressure at the inlet and outlet. It can be seen that the overall rising trend of the outlet static pressure curve is similar to the impeller speed curve, while the inlet static pressure curve always maintains a stable level during the startup process, and the outlet static pressure is always higher than that of the inlet during the startup. The impeller speed rises extremely rapidly at the beginning of the startup, then increases slowly, and finally stabilizes. The total time of startup is 1.0s, and the transient rotational speeds are 1253.764 r/min and 1398.273 r/min at 0.3s and 0.5s, respectively, which have reached 86.58% and 96.56% of the speed after startup stabilization, and it can be seen that the rise of the rotational

Global Digital Central
ISSN: 2151-8629

speed curve is very small after 0.5s. The transient rotational speed at the completion of the startup is about 1448.155r/min, and there is a small difference between the measured speed and the design speed after stabilization, which can be attributed to the voltage instability during the experiment.

The rising trend of the static pressure curve at the pump outlet is similar to that of the speed curve. The rate of rising is high in the early stage of the startup, then gradually slows down and eventually the curve rises to a relatively stable level. The difference is that the rise is slow at the beginning of the startup stage, and the static pressure curve at the outlet always shows obvious regular fluctuations throughout the startup. The increase rate of the outlet static pressure curve is very small within 0.022s at the beginning, and the transient pressure at 0.022s is about 2.195kPa, and then it goes through a rising course from fast to slow. At the same time points, i.e., 0.3s and 0.5s, the transient values of the outlet static pressure are about 63.953 kPa and 82.066 kPa, reaching 72.1% and 92.53% of the final average value, respectively. It can be seen that there is a significant delay compared to the time required for the rotational speed curve to become relatively stable. In addition, it can be found that with the gradual increase of impeller rotational speed, the fluctuation of the outlet static pressure curve becomes more obvious, and the maximum fluctuation is about 10.620kPa. The reason for this phenomenon is that as the impeller rotational speed increases, the fluid flow rate in the pump also increases rapidly, constantly impacting the volute, which leads to the rotor-stator interaction between the impeller and the volute more and more obvious.

On the contrary, the static pressure curve at the inlet is almost not affected by the rotational speed. During the whole startup process, the fluctuation of the inlet static pressure curve is extremely small and almost always remains at a stable level, corresponding to an average static pressure value of about 0.360 kPa. It is not difficult to find that the outlet static pressure value is always higher than that at the inlet. The difference between the two increases gradually with the increase of impeller speed, and the maximum difference reaches 92.717kPa. Compared the curves in Fig. 4 (a) with the reference (Zhang *et al*., 2017), it can be seen that the fluctuation of the inlet static pressure curve is obvious in forward startup, while it is always smooth in reverse startup without any significant fluctuation, and the mean value of the inlet static pressure curve is higher than that in forward startup.

Fig. 4 (b) shows the comparison of the rotation speed curve with the dynamic pressure of the inlet and outlet. Similar to the static pressure, the dynamic pressure at the outlet is always higher than that at the inlet during the entire startup, and there is an obvious shock in the outlet dynamic pressure curve. There are fluctuations of different magnitudes in the inlet and outlet dynamic pressure curves, the reason for this phenomenon is also mainly due to the rotor-stator interaction in the pump. It can be seen that the rising trend of the outlet dynamic pressure curve is obviously different from the rotational speed curve. Firstly, it goes through a rising process from slow to fast, and then gradually decreases to fluctuate around the stable value after reaching the peak, and the dynamic pressure shock is about 0.06kPa. Within 0.074s of the initial startup, the rise of the outlet dynamic pressure curve is extremely small, and the transient dynamic pressure value is about 0.023kPa at this moment.

As the impeller rotational speed increases, the outlet dynamic pressure curve also gradually accelerates. In particular, there is a significant increase in the increase rate at 0.241s, with a transient dynamic pressure value of about 0.281kPa. And then the increase rate gradually slowed down, and the shocking phenomenon appears. It reaches the maximum value at about 0.369s, which is also the maximum value of the dynamic pressure at the outlet during the whole startup, and the transient dynamic pressure is about 0.572kPa. Thereafter, the dynamic pressure curve at the outlet shows an overall decreasing trend, but there is also a very small increase from 0.435s to 0.5s, and the transient dynamic pressure values corresponding to the two time points are 0.538kPa and 0.553kPa, respectively. Finally, it drops to a relatively stable state at about 0.597s, and the average value after stabilization is about 0.512kPa. It can be seen that the change of the curve fluctuation amplitude is small, and the maximum fluctuation amplitude is about 0.012 kPa.

The trend of the inlet dynamic pressure curve with time is similar to the rotational speed curve, but the rise of the inlet dynamic pressure is very small within 0.050s of the startup, and the transient dynamic pressure value is about 0.005kPa at 0.050s. In the middle and later stages of the starting process, the increase rate of the curve is very small. At 0.3s and 0.5s, the corresponding transient dynamic pressure values are about 0.135kPa and 0.179kPa, reaching 68.96% and 91.13% of the final average, respectively. Compared with the time when the speed curve tends to be stable, there is also a lag. During the whole startup process, the inlet dynamic pressure curve also fluctuates, but the degree of fluctuation is significantly smaller than that of the outlet dynamic pressure curve. By comparing these with the corresponding curves in reference (Zhang *et al*., 2017), it is found that forward or reverse rotation has almost no effect on the dynamic pressure curve, the time points of the characteristic changes in the curves are basically the same, with basically similar line shapes and values of the curves.

By comparing Figs. 4 (a) and 4 (b), it can be found that the static pressure value at the outlet is much higher than the dynamic pressure at the outlet. Combining the above data, it can be seen that the dynamic pressure value at the outlet after the stabilization is only 0.58% of the static pressure value at the outlet. In addition, the fluctuation of the static pressure at the outlet is also much larger than the dynamic pressure curve at the outlet, also the maximum fluctuation of the dynamic pressure is only 0.11% of that of static pressure.

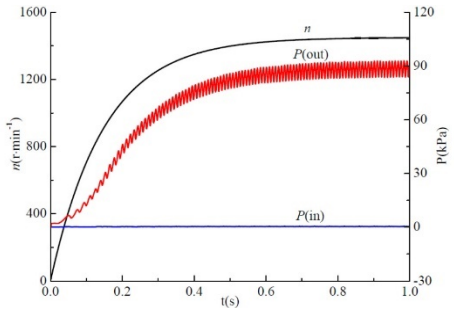

(a) Static pressure

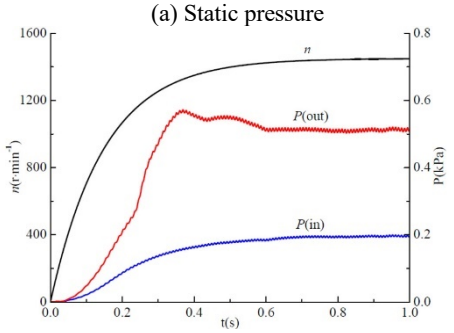

(b) Dynamic pressure

Fig. 4 Pressure of pump inlet and outlet during the reverse startup

Fig. 5 (a) shows the comparison between the rotational speed curve and the total pressure curve at the inlet and outlet. The total pressure is the sum of the values of static and dynamic pressure. By comparing Figs. 4 (a) and 4 (b), it is easy to see that the dynamic pressure at the outlet is much smaller than the static pressure value at the outlet and accounts for a very small percentage constituting the total outlet pressure, so the total pressure curve at the outlet in Fig. 5 is almost the same as the static pressure curve at the outlet in Fig. 4 (a). Within 0.023s after the reverse startup, the total pressure curve at the outlet rises very little due to the small flow in the pump, and the transient pressure value is only about 2.246kPa at this moment. Then it rises rapidly, and the corresponding transient total pressure values are about 64.501 kPa and 86.488 kPa at 0.3s and 0.5s, reaching 72.38% and

97.05% of the average total pressure after the startup stabilization, respectively. This indicates that in the middle and late stages of the reverse startup, the impeller rotational speed and the flow in the pump have been basically stable, so the total pressure curve at the outlet of the centrifugal pump is also relatively stable, fluctuating in a very stable range with a relatively constant average value of about 89.114kPa.

In addition, it can also be found that the fluctuation of the total pressure curve at the outlet also increases significantly with the increase of the rotational speed, then remains stable. This is because the rapid rise of impeller rotational speed in the early startup phase will cause the rotor-stator interaction in the pump to become more intense. The maximum fluctuation amplitude is about 10.255 kPa, which is slightly smaller than that of the outlet static pressure curve. While the static and dynamic pressure curves at the pump inlet are similar in value, and are very tiny compared to the static pressure at the outlet. Therefore, the curve in the figure of the total pressure is almost always stable, and the average value of the total pressure at the inlet is about 0.507kPa during the reverse startup. This is significantly different from the forward startup in reference (Zhang *et al*., 2017). The fluctuation of the total inlet pressure during the forward startup is significantly larger than the fluctuation of the total outlet pressure. In contrast, the inlet total pressure curve hardly fluctuates compared to the outlet total pressure curve during the reverse startup.

The time derivative curves of the impeller rotational speed and the total pressure at the inlet and outlet during the reverse startup are shown in Fig. 5 (b). It is easy to see that the trends of the latter two curves are significantly different from the former. During the startup, the time derivative of the impeller rotational speed gradually decreases, the decrease rate is from fast to slow, and the curve is very smooth. But there are always large fluctuations in the time derivative curves of inlet and outlet total pressure. At the beginning of the startup, the time derivative curves of the total pressure at both the outlet and the inlet of the centrifugal pump have local extreme values respectively, then decrease extremely fast and start to fluctuate after maintaining stability for a very short time. The time derivative curve of the total pressure at the outlet decreases from 2230.03 to 23.19 within the initial 0.005s. And then about until 0.021s, the time derivative of total outlet pressure is almost a horizontal straight line. This is reflected in Fig. 5(a), i.e., the total outlet pressure curve changes approximately linearly. Thereafter, the fluctuation amplitude of the total pressure time derivative curve at the outlet gradually increases.

Until about 0.5s, the curve fluctuation amplitude is still slightly increasing, but the fluctuation range has been relatively stable, and the maximum magnitude of fluctuation during the startup process is about 7014.95. Although the time derivative of the total pressure at the inlet is also extremely high at the beginning of the startup, it is much smaller in value than that of the total pressure at the outlet. Within the first 0.005s of startup, the time derivative of the total inlet pressure drops rapidly from 63.22 to 0.81. It is easy to see that in the initial stage of the startup, the time derivative curve of the total import pressure is relatively chaotic, with irregular fluctuations. This may be due to the rapid increase in impeller rotational speed in the initial stage of the reverse startup, the internal flow of the pump is turbulent and violent. After about 0.2s, the periodicity and regularity of the curve gradually become obvious, but the amplitude of the fluctuation is still changing. In the middle and later stages of the startup, there is still a small change in the fluctuation amplitude, but the period stability of the curve is obvious. The period for the occurrence of a feature change also decreases and stabilizes with time, and the period after stabilization is about 0.042s. The maximum magnitude occurs at about 0.945s with a value of about 209.21.

Comparing Figs. 5 (a) and 5 (b), although the rising trend of the outlet total pressure curve has some similarity with the rotational speed curve, the difference in the trend is very obvious in the time derivative curve.

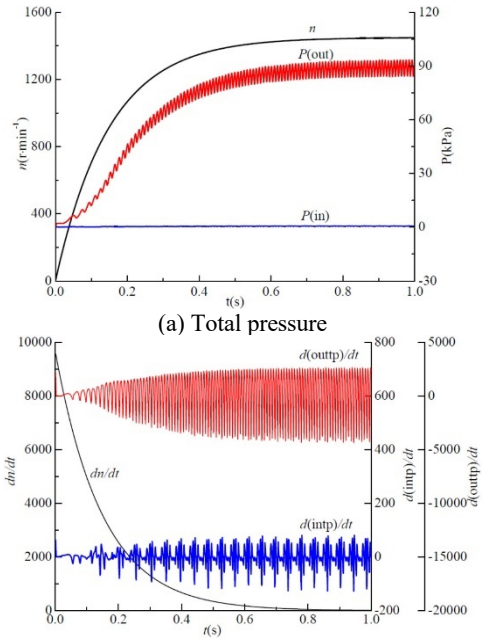

(a) Total pressure

(b) The time derivative of the total pressure

Fig. 5 Total pressure of pump inlet and outlet during the reverse startup

The transient hydraulic performance curves of the centrifugal pump during the reverse startup are shown in Fig. 6. It can be found that the rising trends of the transient flow rate, transient head, and transient shaft power curves are generally similar to the speed curves, but there are different degrees of difference, respectively. Except for the rotational speed curve, the other three hydraulic performance curves show obvious fluctuations during the rise, and the fluctuation amplitude of each curve is different. In addition, in the initial startup stage, the increase rate of flow rate, head, and shaft power curve is slower compared with the speed curve, especially in the rising process of the head and the shaft power curve. In the middle of the startup, the three curves experience acceleration, then gradually slow down and eventually reach relatively stable respectively. Among them, the trend of the transient flow curve is most similar to the rotational speed curve, indicating that the rotational speed has a greater degree of influence on the flow rate. The increase rate of the flow curve is slow until about 0.031s, and the transient flow value is about 0.26 m^3/h at 0.031s, which is due to the fact that the whole water and the impeller are stationary before the start. Then the flow rate increases rapidly.

At about 0.3s, there is a gradual and obvious slowdown of the increase rate, and the transient flow value at this time is about 3.60 m^3/h, which has reached about 82.94% of the average value of the flow rate after the startup stabilization. The small amplitude rise phase continues until about 0.653s, with a transient flow rate of about 4.32 m^3/h. It can be seen that the flow curve is very stable after 0.653s. Although it is still accompanied by certain amplitude fluctuations, the average value remains almost the same, because the rotational speed is basically stable at this time. The average value of the flow rate during the time period from 0.653s to the completion of the reverse start is about 4.32 m^3/h. It is easy to see that the trend of the head curve and the fluctuation characteristics are almost the same as the total pressure curve at the outlet in Fig. 5 (a), which is due to the fact that the total pressure at the outlet is always much larger than the inlet, and the pressure value at the outlet plays an absolutely dominant role in the calculation of the head. The head curve is similar to the rise of the rotational speed curve in the middle and late stages of the startup, because essentially the head is also largely affected by the rotational speed. The increase rate of the head curve is relatively slow until about 0.022s, and the transient head value is about 0.414m at this moment. Then the head rises rapidly until about 0.655s, and the overall trend of the curve rises slowly. Although the curve fluctuation amplitude is large, the range is relatively stable, at this

Global Digital Central
ISSN: 2151-8629

moment the transient head is about 9.019m, and the error of the average value of the final head is already within 2%.

It can also be found from Fig. 6 that the shaft power curve has almost no fluctuation and increases linearly during the initial 0.066s of the startup period, and the transient shaft power value is about 28.793W at 0.066s. Thereafter, the shaft power curve begins to fluctuate with increasing amplitude and the overall increase rate is higher than before. About 0.7s after the startup, the overall level of the shaft power curve is stable and fluctuates within a certain range. The transient shaft power at 0.7s is about 290.018W, which has reached about 97.72% of the average shaft power at startup completion. There are also fluctuations in the amplitude of the shaft power curve during the startup, but it is obvious that this fluctuation increases slowly with time, and the amplitude of the fluctuation is gradually stable. In addition, even if the rotational speed curve is basically constant, there are still very obvious fluctuations in the head and shaft power curve, which is due to the rotor-stator interaction in the pump at a high speed. Overall, at the time points of 0.300s and 0.500s, the values of rotational speed have increased to 86.58% and 96.56% of the final stable values, respectively. The transient flow rate reaches 82.94% and 95.83% of the final stable value at the corresponding time points, and the transient head is 72.92% and 92.82% of the final stable mean value, respectively. The transient shaft power is 63.05% and 90.79% of the final stable level, respectively. It can be seen that these three hydraulic performance parameters have certain time lags compared to the change in the rotational speed curve. The lag of the shaft power is the largest, the head is the second largest and the flow rate is the smallest.

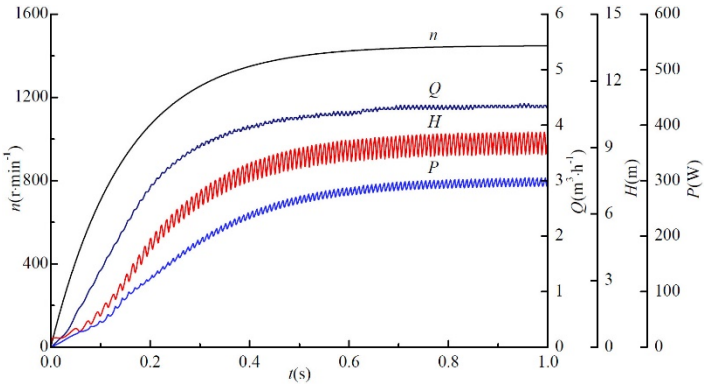

Fig. 6 Transient hydraulic performance of the reverse startup

The time derivatives of the transient hydraulic performance during the reverse startup are shown in Fig. 7. Compared with Fig. 6, although the increase trend of the flow and head curves is roughly similar to the rotational speed curve, the corresponding time derivative curves are significantly different and are always accompanied by fluctuations of different magnitudes during the change. It can be seen that the time derivative curve of the head drops almost instantly from a large value to a relatively low level within the initial 0.003s of the startup, with a large value of about 221.1. The transient head time derivative at 0.003s is about 5.68. For 0.003s < t < 0.02s, the curve is nearly a horizontal straight line, indicating that the trend of head change during this time is nearly linear in form with very small fluctuations. The time derivative curve of the head starts to fluctuate after 0.02, and the magnitude of the fluctuation gradually increases, with the maximum fluctuation being about 701.5, which is slightly smaller than 707.1 in the forward opening (Zhang *et al*., 2017).

After about 0.5s, the fluctuation range of the time derivative curve of the head is gradually stabilized. Although the fluctuation is still increasing, the increase is already very small. Compared with Fig. 5 (b), it can be seen that the trend of the time derivative curve of the head is basically the same as the time derivative curve of dynamic pressure at the outlet. This is also due to the fact that the dynamic pressure at the outlet plays an absolutely dominant role in the calculation of the head. Different from the time derivative curve of the head, the time derivative curve of the flow rate increases firstly and then decreases at the beginning of the startup phase, then gradually stabilizes, and the whole startup process is accompanied by large fluctuations. The reason for the smaller value of the time derivative curve of the flow in the initial phase of the startup is mainly due to the stationary state of the whole water and the impeller before the startup.

At about 0.165s, the time derivative curve of the flow rate rises to a local extreme value of about 24.9, and then decreases slowly to reach a periodic stable state with an average value of 1.21 in the relatively stable state. It can be seen from the figure that the amplitude of the fluctuation of the time derivative curve of the flow rate increases gradually until about 0.3 s. At 0.3 s, there is a significant abrupt change in the amplitude of the fluctuation, with a sudden increase in value from 27.22 to 36. Then the amplitude of fluctuation remains constant at 36, which is consistent with the amplitude of the time derivative curve of the flow rate variation at forward startup in reference (Zhang *et al*., 2017). It is worth noting that at about 0.6s, the rotational speed curve has basically stabilized, but the time derivative curve of the flow rate still has large fluctuations. It can be seen that the fluctuation of flow rate always exists in the whole startup process. But at different time stages, it shows different fluctuation characteristics, i.e., the fluctuation amplitude increases gradually in the earlier stages and is very stable in the middle and later stages of the startup. The main reason for this phenomenon is also the rotor-stator interaction in the centrifugal pump. In the usual numerical calculation, if the impeller speed has been basically constant during the startup, the flow rate is generally regarded as a constant value. As can be seen from Fig. 6, the flow rate fluctuation is really very small after the rotational speed is stable.

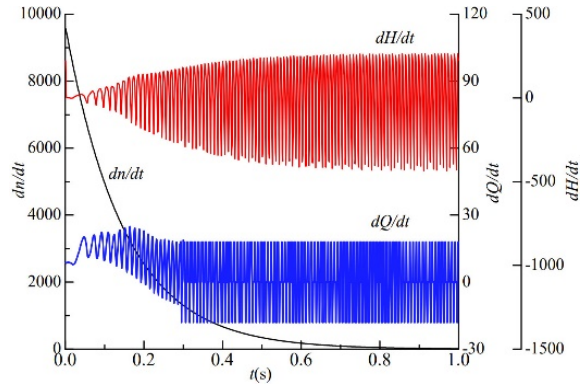

Fig. 7 Time derivatives of the transient hydraulic performance of the reverse startup

During the reverse startup, the rotational speed changes rapidly and the performance parameters change accordingly. In order to exclude the effect of the rotational speed, the reverse startup process is described in terms of dimensionless flow rate, dimensionless head and dimensionless power. The three are defined as follows

$$\begin{cases} \phi(t) = Q(t) / \pi D_2 b_2 u_2(t) \\ \psi(t) = 2gH(t) / u_2^2(t) \\ \Phi(t) = P(t) / \rho D_2^2 u_2^3(t) \end{cases} \quad (5)$$

where $u_2(t)$ is the transient circumferential velocity at the impeller outlet, whose expression is $u_2(t) = \pi D_2 n(t) / 60$.

Fig. 8 shows the time history of the evolution of the transient dimensionless flow, dimensionless head and dimensionless shaft power during the reverse startup. From the figure, it can be found that only the rising trend of the dimensionless flow curve among the three dimensionless parameters is similar to the rotational speed curve. But the other two curves are obviously different from the rotational speed curve. And during the reverse startup, the curves of these three dimensionless parameters are accompanied by fluctuations of different magnitudes. Among them, the dimensionless flow curve rises extremely

rapidly in the earlier phase of the startup, For t<0.009s, the dimensionless flow curve has no obvious fluctuation and grows almost linearly, with the value rising from 0 to 0.0055 in 0.009s, which is about 27.8% of the final stable average. Then its increase rate has a tendency to gradually slow down, and the curve has basically stabilized at 0.3s and 0.5s, with values of about 0.0189 and 0.0195, reaching about 95.54% and 98.58% of the final stable average value, respectively. The percentages corresponding to the rotational speed curve at these two time points are 86.58% and 96.56%, respectively, which shows that the time of stabilization of the dimensionless flow curve is significantly advanced with respect to the rotational speed curve.

It can also be found that there are extreme values of the dimensionless head curve at the initial stage of the startup, which is caused by the high rotational acceleration of the impeller at the beginning of the startup and the impact on the stationary water body. Then the dimensionless head drops rapidly to a minimum value, and finally rises slowly to a relatively stable state. It can be seen that the dimensionless head curve drops to the minimum value at about 0.082s, and the minimum value is about 0.792. Then it slowly rises, at about 0.3s after startup, the value of the dimensionless head is about 1.193, which is about 97.03% of the average value after the stabilization. For 0.3s to 0.5s, the overall rise of the dimensionless head curve is extremely small. The transient dimensionless head value is about 1.222 at 0.5s, which has reached about 99.39% of the final stable value.

In the latter stage of the startup, the dimensionless head curve fluctuates within a nearly constant range, with an average value of about 1.225. Compared to the dimensionless flow and rotational speed curves, the dimensionless head curve stabilizes earlier. For the dimensionless shaft power curve, there are also extreme values at the initial stage of the startup. However, unlike the dimensionless head curve, its rapid decline is accompanied by fluctuations. It can be seen that the amplitude of the fluctuations in this drop is decreasing. At about 0.122s, it drops to a local minimum value of about 0.0072. After keeping the horizontal fluctuation for a very short time, it decreases again, and the decreasing rate gradually slows down with time, finally it has basically reached stability at about 0.25s. At this time, the value of the dimensionless shaft power is about 0.0065, and the average value of the curve in the subsequent time is also 0.0065. In the process of the reverse startup, the dimensionless shaft power curve is also always accompanied by fluctuation, and the fluctuation decreases continuously with the increase of the rotational speed. The decrease of fluctuation amplitude is very obvious in the early stage of the startup, and the amplitude is almost unchanged in the later stage. In addition, the dimensionless shaft power curve is the first to stabilize compared with the other two dimensionless parameters and the rotational speed curve.

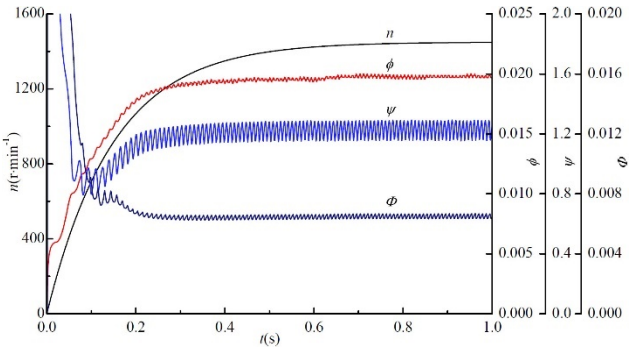

Fig. 8 Transient dimensionless parameters during the reverse startup

Fig. 9 and Fig. 10 show the time history of the hydraulic efficiency and the impeller dynamic reaction force variation during the reverse startup, respectively. And the hydraulic efficiency is defined as follows

$$\begin{cases} P(t) = 2\pi M(t)n(t)/60 \\ \eta(t) = \rho g Q(t)H(t)/P(t) \end{cases} \quad (6)$$

where M(t) is the transient impeller torque.

From Fig. 9, it can be found that the rising trend of the hydraulic efficiency curve is obviously different from that of the rotational speed curve. The hydraulic efficiency curve is fluctuating in the early stage of the startup. It has reached a more stable state in the middle and late stages, accompanied by periodic fluctuations, and the magnitude of fluctuations is relatively stable. About 0.005s ago, the hydraulic efficiency curve rises extremely fast, and then quickly resumes the normal fluctuating rise, and the transient hydraulic efficiency at 0.005s is about 2%. For 0.005s < t < 0.3s, the hydraulic efficiency curve rises rapidly, with gradually decreasing fluctuations. At 0.3s, the hydraulic efficiency is about 35.37%, which is about 96.59% of the final average. It has basically reached a stable state, and thereafter the rise is very small. At 0.5s, the hydraulic efficiency is about 36.33%, which has reached 99.21% of the final average. Compared with the rotational speed curve, at the same two moments, the rotational speed reaches 86.58% and 96.56% of the final steady state value respectively, and it can be seen that the hydraulic efficiency is significantly earlier compared to the time when the speed reaches the steady state. In the middle and late stages of the reverse startup, the average of the hydraulic efficiency curve is almost constant at 36.62%. At about 0.527s, the maximum fluctuation amplitude occurs and the value is about 4.57.

Fig. 10 shows the time history of the evolution of the impeller dynamic reaction force and the rotational speed during the reverse startup. During the running of the radial centrifugal pump, the fluid enters the impeller from the axial direction and flows out from the radial direction, the fluid direction changes dramatically. Combined with the momentum equation, the dynamic reaction force is generated on the inner surface of the back cover of the impeller. As can be seen from the figure, the evolution course of the dynamic reaction force curve with time differs more significantly from the rotational speed curve. The dynamic reaction force of the impeller rises rapidly in the initial stage of the startup, accompanied by fluctuations, and the curve is almost irregular. The increase rate slows down in the middle and late stages.

With the stabilization of the rotational speed, the fluctuation of the dynamic reaction force curve obviously shows a periodic law, and finally it is in a more stable state. Before about 0.051s, the dynamic reaction force curve rises rapidly, and the transient dynamic reaction force is about 0.38N at 0.051s. For 0.051s to 0.2s, there are very strong fluctuations in the rising course of the dynamic reaction force curve, in which a local extreme value occurs at about 0.131s with a transient value of about 1.05N. It can be found that after 0.2s, the changing trend of the dynamic reaction force curve shows a gradually obvious periodic law. For about 0.2s to 0.6s, the dynamic reaction force curve increases overall, but the increase rate gradually slows down. Thereafter, the curve still fluctuates regularly, but the average has been relatively stable. This indicates that the dynamic reaction force of the impeller will change drastically in the early stage of the startup because of the rapid increase of the rotational speed. After the rotational speed is gradually stable, the dynamic reaction force shows periodic stability.

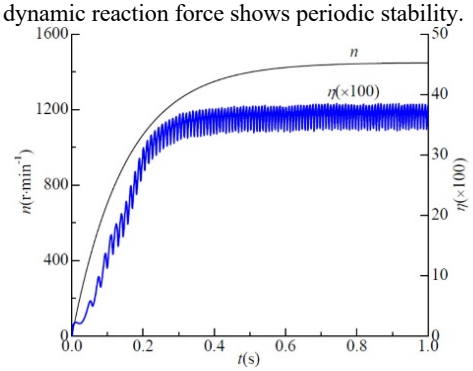

Fig. 9 The rising course of the hydraulic efficiency

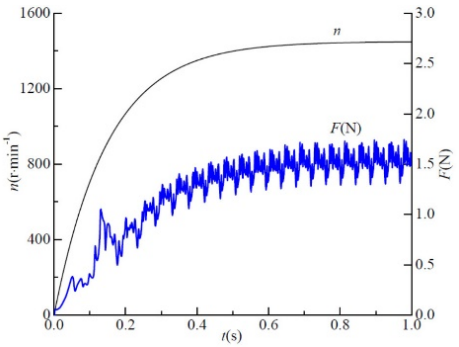

Fig. 10 The rising course of the impeller dynamic reaction force

3.2 Analysis of the Flow Field

Fig. 11 shows the evolution characteristics of the total pressure with time at the mid-section position of the pump during the reverse startup. As is known to all, the essence of the centrifugal pump operation is to convert the input mechanical energy into pressure energy for output, so the impeller rotational speed increases rapidly, resulting in a sharp rise in pressure in the pump. It is easy to see in the figure that the total pressure in the mid-section increases significantly with time. During the reverse startup, the total pressure on the pressure and suction surfaces of the blades is asymmetrically distributed. This is due to the rotor-stator interaction between the asymmetric structure of the volute and the geometrically symmetrical impeller. It can also be seen that the lowest pressure in the mid-section always appears at the inlet of the impeller during the reverse startup, and the range of the low-pressure region also decreases gradually with the increase of the rotational speed, it becomes stable finally.

In addition, as the rotational speed increases, the total pressure always increases gradually along the flow path in the radial direction of the impeller. This is because a larger radius results in a higher linear velocity which generates a larger centrifugal force and Coriolis force. In the same radial position, the total pressure on the suction side of the blade is always lower than the pressure side of the blade. Combined with the impeller rotational speed curve, the transient rotational speed has been nearly stable for t=0.4s. The high-pressure region appears first near the trailing edge at the pressure side of each blade, and then the range of the high-pressure region still gradually expands with the increase of the rotational speed. For t=1.0s, the distribution trend is basically the same as that at 0.4s, with an overall increase in the total pressure value. The maximum value of total pressure appears near the trailing edge of the pressure side of the blade, which is about to pass the tongue of the volute, and the maximum total pressure value is about 111.785 kPa.

It can be found that compared with other positions, the total pressure changes more dramatically near the impeller outlet at the pressure side of the blade, and there are high-pressure areas, this is mainly because of the jet-wake structure at the outlet of the impeller and the rotor-stator interaction. The minimum total pressure value appears near the leading edge at the suction surface of the impeller, and the minimum value is about -8.115kPa, this is also the lowest total pressure value during the reverse startup. This is due to the split flow phenomenon when the fluid enters the impeller inlet, which will lead to a result that a part of the pressure surface at the impeller inlet can not be filled with fluid in time, thus reducing the pressure or even generating negative pressure. As a result, cavitation occurs more easily at the inlet of the impeller than at other positions. It can be seen that the total pressure at the impeller inlet decreases with the increase in speed, so it is necessary to add devices such as induction wheels before the impeller inlet of the centrifugal pump to prevent cavitation. In summary, during the reverse startup, the total pressure in the pump rises significantly with the increase of impeller rotational speed, and the total pressure increases step by step along the impeller flow path.

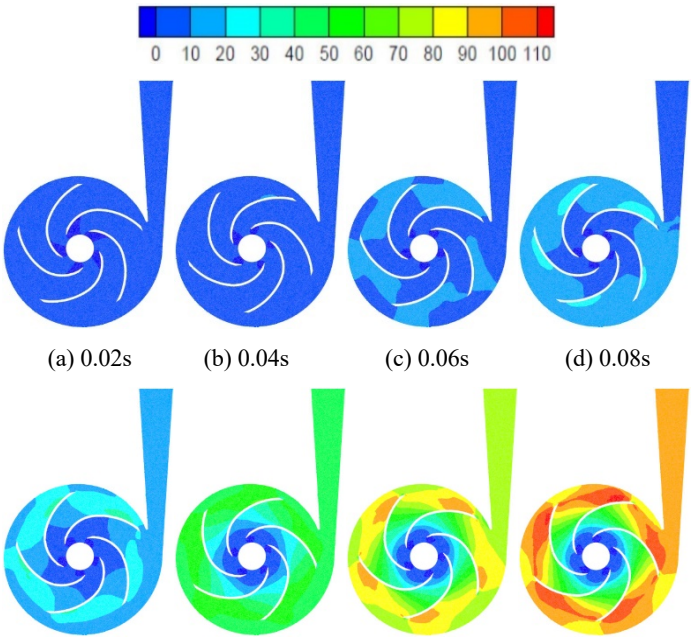

Fig. 11 Evolution characteristics of total pressure during the reverse startup

The change of turbulence energy with time can reflect the development and decline of turbulence during the reverse startup of the centrifugal pump. As can be seen from the figure, the region where the turbulent kinetic energy mainly occurs changes from the outlet of the volute to the flow path of the impeller with time. As shown in Figs 12(a) to 12(e), in the initial 0.08s of the reverse startup, the main area of turbulent kinetic energy occurs at the center of the volute outlet, and a small portion of turbulent kinetic energy is distributed near the leading edge of each blade. During this time, the turbulent kinetic energy at the outlet of the volute gradually decreases continuously and disappears at 0.2s. It can be seen that the distribution of the turbulent kinetic energy near the outlet of the volute shows a trend of decreasing step by step from the outlet to the inside with the increase of the impeller speed within 0.1s after the startup, but the region of the turbulent kinetic energy at the leading edge of each blade is slowly increasing.

Overall the turbulent kinetic energy at the leading edge of the blade has a low value, with a small occurrence area, and it has a weak symmetry about the impeller center. At 0.1s, it is obvious that there is a weak symmetry of the turbulent kinetic energy distribution region about the impeller center, which is mainly caused by the interaction between the asymmetric structure of the volute and the central symmetric structure of the impeller during the startup. From 0.1s to 0.2s, it can be found that the turbulent kinetic energy in the impeller flow path is firstly generated at the pressure surface and the trailing edge of each blade, and then gradually spreads to the whole flow path. The turbulent kinetic energy at the leading edge of the blade is gradually transferred to the front part of the suction side of the blade, but there is almost no distribution of the turbulent kinetic energy at the front part of the pressure side, and this feature is approximately symmetric about the axis. After 0.2s, the turbulent kinetic energy is mainly concentrated in the flow path of the impeller.

At the same time, a very small part of turbulent kinetic energy is distributed on the inner surface of the volute. After the speed is basically stable, the turbulence kinetic energy gradually decreases from the pressure side of the blade to the suction side of the next blade in the circumferential direction of the impeller. At 1.0s, there is an obvious region of higher turbulent kinetic energy at the central position immediately adjacent to the pressure surface of the blade, and the maximum value is about 0.58m^2/s^2. In the radial direction, the turbulent

Global Digital Central
ISSN: 2151-8629

kinetic energy near the leading edge and trailing edge of the blade is small, and gradually increases toward the center of the impeller. And at the same radial position, the turbulent kinetic energy of the pressure side is always higher than the suction side of the blade.

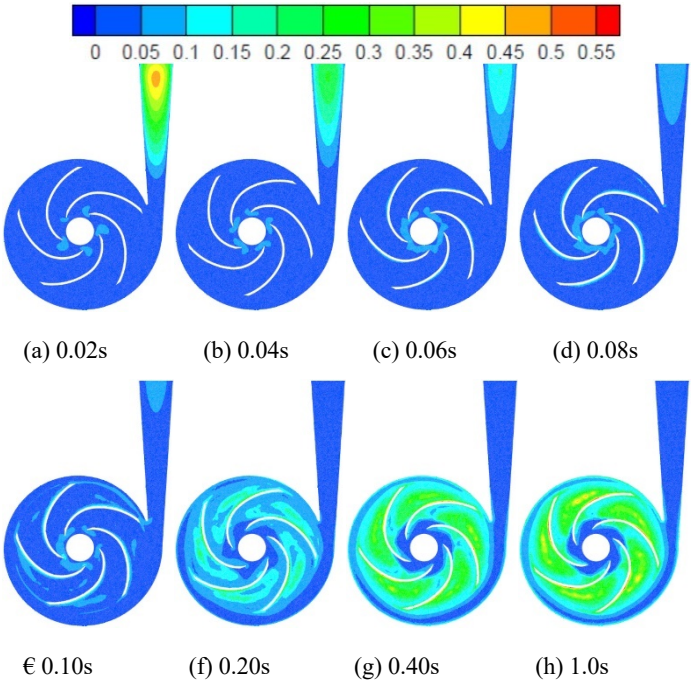

(a) 0.02s (b) 0.04s (c) 0.06s (d) 0.08s

€ 0.10s (f) 0.20s (g) 0.40s (h) 1.0s

Fig. 12 Evolution characteristics of the turbulent kinetic energy during the reverse startup

The evolution characteristics of the turbulent dissipation rate with time on the mid-section of the centrifugal pump during the reverse startup are shown in Fig. 13. The turbulent dissipation rate is used to characterize the loss of turbulent kinetic energy by unit mass of fluid in unit time. From the following set of figures, it can be found that the turbulent dissipation rate basically does not appear in the mid-section position before 0.1s of the startup. Until 0.1s, the turbulent dissipation rate only exists in a very small area in the center of the blade pressure surface at the mid-section position, and the maximum value is about 160.502m^2/s^3. After 0.2s, the value and distribution area of the turbulent dissipation rate increase slowly. In the radial direction of the impeller, the turbulent dissipation rate is mainly distributed in the pressure and suction sides of each blade, and the area is still very narrow. Until about 0.4s, the rotational speed of the impeller has been basically stable, and a very small part of the turbulent dissipation rate starts to appear close to the trailing edge of the blade and the inner wall of the volute.

Especially, there is no turbulent dissipation rate in the region near the front part of the blade at all times during the startup, which indicates that the turbulent kinetic energy values are basically unchanged in this region. In the same radial position of the blade, the turbulent dissipation rate at the pressure side of the blade is always higher than that at the suction side. In the circumferential direction of the impeller, the turbulent dissipation rate is stepped around the blade, and the value of the turbulent dissipation rate is higher near the center of the pressure and suction sides of the blade, and gradually decreases at the leading edge and trailing edge, respectively. By comparing Figs. 13(g) and 13(h), it can be seen that the distribution area and the value of the turbulent dissipation rate at 0.4s are already closer to those at 1.0s. The maximum value of the turbulent dissipation rate is 798.343m^2/s^3 at 0.4s and 928.612m^2/s^3 at 1.0s. It is mainly due to that the transient rotational speed of the impeller at 0.4s has reached 93.17% of the design rotational speed, and the internal flow of the pump has been more stable.

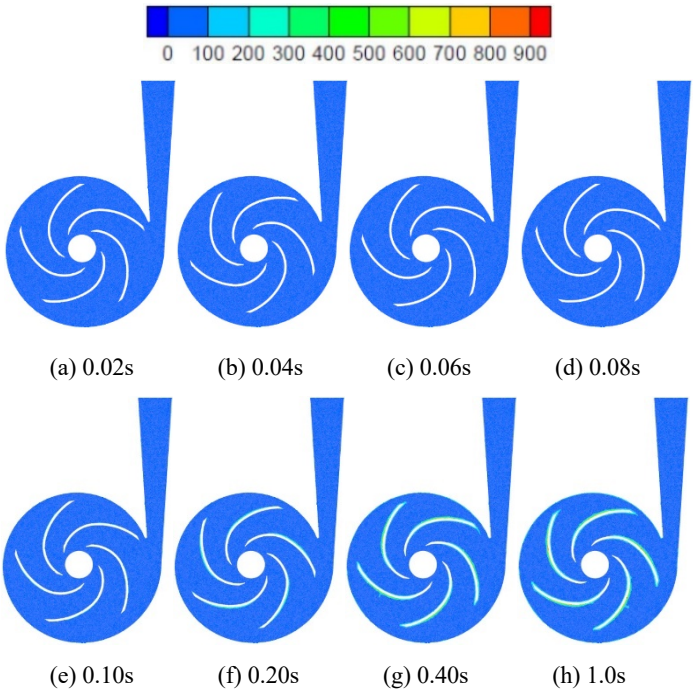

(a) 0.02s (b) 0.04s (c) 0.06s (d) 0.08s

(e) 0.10s (f) 0.20s (g) 0.40s (h) 1.0s

Fig. 13 Evolution characteristics of the turbulent dissipation rate during the reverse startup

3.3 Discussion

In this paper, numerical simulations are carried out for the reverse startup of a centrifugal pump in the case of operation error based on the established circulation piping system, and the reverse startup characteristics of the pump model are obtained. Although the above work has basically reached the expected goal, there are aspects that can be further improved.

(1) In this paper, the unstructured mesh is used for the main over-flow components of the centrifugal pump model, and it would be more reliable if the structured mesh is applied and compared with the meshing scheme used in this paper, and then the optimal meshing scheme is determined for the numerical simulation.

(2) For the analysis of the internal flow field, the distribution clouds at other cross sections should be added, as well as more time nodes can be divided before the impeller rotational speed stabilizes, in order to observe more clearly the flow and the energy dissipation in the pump during the reverse startup.

(3) The similitude law is an important theoretical basis in the design process of vane pumps. It is commonly used to predict the effect of parameters such as impeller rotational speed or impeller diameter on the hydraulic performance of a centrifugal pump during steady running. According to the similitude law of centrifugal pumps mentioned in the literature (Zhang *et al*., 2016), the equation (7) for the theoretical head of a centrifugal pump during the reverse startup can be further derived.

$$H_t = H_0\left(\frac{Q}{Q_0}\right)^2 \tag{7}$$

Where, H_0, Q_0 are the head and flow rate values after the reverse startup is completed, which are replaced by the average value after the startup is basically stabilized in this paper. Q is the transient flow rate at each moment of the startup process, and H_t is the theoretical head calculated according to the similitude law.

Fig. 14 shows the transient head-flow curve (H-Q) from the numerical simulation of the reverse startup and the theoretical head-transient flow curve (H_t-Q) calculated by the similitude law, respectively. By comparing the two curves, it can be found that the overall rising trend of the two is approximately the same, but the H-Q

curve is always accompanied by fluctuations. In the early startup stage, when the flow rate is small, the value of the transient head curve is above the theoretical head, and the difference between the two is large. This is mainly due to the obvious transient characteristics of the pump in the early startup stage, the transient head and flow rate change rapidly, and the two curves are accompanied by large fluctuations, so the *H-Q* curve fluctuates greatly. However, in the middle and later stages of the startup, the difference between the two curves gradually decreases, and the *H-Q* curve approximately fluctuates up and down with the H_t-*Q* curve as the center. In summary, the similitude law of centrifugal pumps does not apply in the early stage of the reverse startup, but as the rotational speed stabilizes, the transient flow and head also gradually tend to be stable. Therefore, in the late stage of the startup, the similitude law can be applied to the performance prediction of the centrifugal pump.

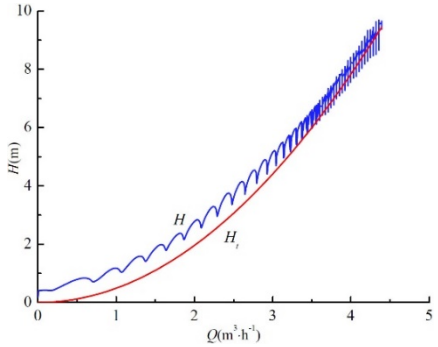

Fig. 14 Transient head, theoretical head-flow rate curves

4. CONCLUSION

(1) It is obvious that the influence of the forward and reverse rotation on the static pressure at the inlet of the centrifugal pump. In the case of the forward startup, the static pressure curve at the inlet first falls, then rises, and there are very large regular fluctuations in the amplitude. While the inlet static pressure curve does not fluctuate during the reverse startup, and it always remains horizontal.

(2) There are certain time lags in the hydraulic performance parameters curves to a steady state compared to the rotational speed curve, and the largest lag is the shaft power, followed by the head and the smallest is the flow rate.

(3) The three dimensionless curves show significantly different evolutionary characteristics. At the initial stage of the startup, the dimensionless head and the dimensionless shaft power curves have maximum values, which drop rapidly. This is mainly due to the high rotational acceleration of the impeller at the initial startup, which is caused by the impact on the stationary water body. Then the dimensionless head gradually rises to stability, while the dimensionless shaft power continues to decline until stability; The dimensionless flow rises rapidly in the first period and then flattens out.

(4) The region where the turbulent kinetic energy mainly occurs changes from the outlet of the worm housing to the flow path of the impeller. The region near the leading edge of the blade, where there is no turbulent dissipation rate at all times during the startup, and there is almost no change in the value of turbulent kinetic energy in this region.

(5) The similitude law of centrifugal pumps is obviously not applicable in the early stage of the reverse startup, and in the later stage, the similitude law is basically applicable to the performance prediction of the centrifugal pumps.

ACKNOWLEDGEMENTS

The research was financially supported by the "Pioneer" and "Leading Goose" R&D Program of Zhejiang (Grant No. 2022C03170), Science and Technology Project of Quzhou (Grant No.2022K98), and Zhejiang Provincial Natural Science Foundation of China (Grant No. LZY21E060001).

NOMENCLATURE

n	the rotational speed (r/min)
n_{max}	the maximum rotational speed (r/min)
t	time (s)
Q	the flow rate (m^3/h)
H	the head (m)
P	the transient shaft power (W)
P(in)	the pressure at the inlet (kPa)
P(out)	the pressure at the outlet (kPa)
u_2(t)	the transient circumferential velocity at the impeller outlet (m/s)
M(t)	the transient impeller torque (N·m)
H_0	the head after the reverse startup is completed (m)
Q_0	the flow rate after the reverse startup is completed (m^3/h)
H_t	the theoretical head (m)

Greek Symbols

φ	the transient dimensionless flow rate
ψ	the transient dimensionless head
Φ	the transient dimensionless shaft power
η	the hydraulic efficiency

REFERENCES

Chen, S.Y., Li, C.F., Qu, Y.P., et al., 2006, "Transient Hydraulic Performance of a Centrifugal Pump During Rapid Startup Period," *Jouranl of Engineering Thermophysics*, **27**(5), 781-783. https://doi.org/10.3321/j.issn:0253-231X.2006.05.019

Cheng, L., and Zhang, Y.L., 2022, "Self-coupling Numerical Calculation of Centrifugal Pump Startup Process," *Frontiers in Heat and Mass Transfer*, **18**(26), 1-6. http://dx.doi.org/10.5098/hmt.18.26

Cheng, L., Zhang, Y.L., and Li, J.F., 2022, "Diagnosis of Centrifugal Pump Speed Fluctuation by Using Vortex Dynamics," *Frontiers in Heat and Mass Transfer*, **19**(32), 1-7. http://dx.doi.org/10.5098/hmt.19.32

Dazin, A., Caignaert, G., and Bois, G., 2007, "Transient Behavior of Turbomachineries: Applications to Radial Flow Pump Startups," *ASME Journal of Fluid Engineering*, **129**(11), 1436-1444. https://doi.org/10.1115/1.2776963

Hu, Z.Y., Wu, D.Z., and Wang, L.Q., 2005, "Transient hydrodynamic performance of centrifugal pump during rapid startup period: Study of explicit characteristics," *Journal of Zhejiang University (Engineering Science)*, **39**(5), 605-608, 622. https://doi.org/10.3785/j.issn.1008-973X.2005.05.001

Lefebvre, P.J., Barker, W.P., 1995, "Centrifugal Pump Performance During Transient Operation," *ASME Journal of Fluid Engineering*, **117**(2), 123-128. https://doi.org/10.1115/1.2816801

Li, Z.F., Wu, D.Z., Wang, L.Q., et al., 2010, "Numerical Simulation of the Transient Flow in a Centrifugal Pump During Startup Period," *ASME Journal of Fluids Engineering*, 132(8), 1-8. https://doi.org/10.1115/1.4002056

Global Digital Central
ISSN: 2151-8629

Thanapandi, P., Prasad, R., 1995, "Centrifugal Pump Transient Characteristics and Analysis Using the Method of Characteristics," *International Journal of Mechanical Sciences*, **37**(1), 77-89. https://doi.org/10.1016/0020-7403(95)93054-A

Tsukamoto, H., Ohashi, H., 1982, "Transient Characteristics of a Centrifugal Pump During Startup Period," *ASME Journal of Fluids Engineering*, **104**(1), 6-13. https://doi.org/10.1115/1.3240859

Wang, L.Q., Li, Z.F., Dai, W.P., et al., 2008, "2-D Numerical Simulation on Transient Flow in Centrifugal Pump During Startup Period," *Journal of Engineering Thermophysics*, **29**(8), 1319-1322. https://doi.org/10.3321/j.issn:0253-231X.2008.08.014

Wu, D.Z., Wang, L.Q., Hu, Z.Y., 2006, "Experimental Study on Explicit Performance of Centrifugal Pump During Rapid Startup Period," *Journal of Engineering Thermophysics*, **27**(1), 68-70. https://doi.org/10.3321/j.issn:0253-231X.2006.01.021

Yakhot, V., Orzag, S.A., 1986, "Renormalization Group Analysis of Turbulence: Basic Theory," *Journal of Scientific Computing*, **1**(1), 1–51.

Zhang, Y.L., Zhu, Z.C., Dou, H.S., et al., 2017, "Numerical Investigation of Transient Flow in a Prototype Centrifugal Pump during Startup Period," *International Journal of Turbo & Jet-Engines*, **34**(2), 167-176. https://doi.org/10.1515/tjj-2015-0064

Zhang, Y.L., Zhu, Z.C., Li, W.G., 2016, "Experiments on Transient Performance of a Low Specific Speed Centrifugal Pump with Open Impeller," *Proceedings of the Institution of Mechanical Engineers Part A, Journal of power and energy*, **230**(7), 648-59. https://doi.org/10.1177/0957650916666452